applied sciences

MDPI

Article

Numerical Analysis of a Dual-Wavelength-Clad-Pumped 3.5 µm Erbium-Doped Fluoride Fiber Laser

Kaidi Cai [1,2], Xin Zhang [1], Lijie Wang [1], Yanjing Wang [1], Huanyu Lu [1], Cunzhu Tong [1,*] and Lijun Wang [1]

[1] State Key Laboratory of Luminescence and Applications, Changchun Institute of Optics, Fine Mechanics and Physics, Chinese Academy of Sciences, Changchun 130033, China; caikaidi17@mails.ucas.ac.cn (K.C.); zhang315xin@ciomp.ac.cn (X.Z.); wanglijie@ciomp.ac.cn (L.W.); wyj_10@lzu.edu.cn (Y.W.); luhuanyu@ciomp.ac.cn (H.L.); wanglj@ciomp.ac.cn (L.W.)

[2] Center of Materials Science and Optoelectronics Engineering, University of Chinese Academy of Sciences, Beijing 100049, China

* Correspondence: tongcz@ciomp.ac.cn

Abstract: The stability and efficiency of a 3.5 µm erbium-doped fluoride fiber is strongly limited by the core pumping setup of a 1976 nm pump. A dual-wavelength-clad-pumped scheme was put forward for a more robust and higher electro-optical efficiency in this paper, and a numerical model was built up to stimulate the fiber. Parameter optimizations were given for both the traditional dual-wavelength pump setup and our new scheme. The results show the possibility of using a laser diode as pump source for the generation of a 3.5 µm laser, and the characteristics were analyzed.

Keywords: fiber lasers; ZBLAN; mid-infrared; numerical mode

Citation: Cai, K.; Zhang, X.; Wang, L.; Wang, Y.; Lu, H.; Tong, C.; Wang, L. Numerical Analysis of a Dual-Wavelength-Clad-Pumped 3.5 µm Erbium-Doped Fluoride Fiber Laser. *Appl. Sci.* **2022**, *12*, 7666. https://doi.org/10.3390/app12157666

Academic Editor: Ju Han Lee

Received: 13 June 2022
Accepted: 27 July 2022
Published: 29 July 2022

1. Introduction

A laser of around 3.5 µm is of particular interest in defence and security, material processing, greenhouse gas monitoring, and spectroscopy [1–4]. Since the introduction of the dual-wavelength pump (DWP) [5], using the $^4F_{9/2} \rightarrow {}^4I_{9/2}$ transition in an erbium-doped fluoride (Er^{3+}:ZrF_4) fiber has become an attractive method for generating a 3.5 µm laser. In 2015, Vincent Fortin et al. reported a watt-level continuous wave (CW) 3.44 µm fluoride fiber laser [6], and the power record increased to 5.6 W [7] and 14.9 W [8] successively.

The DWP scheme requires a 976 nm pump (P_{976}) and a 1976 nm pump (P_{1976}) as shown in Appendix A, Figure A1. Now, the P_{1976} in DWP schemes must be core-coupled to the active fiber to have a sufficient pump absorption rate. Moreover, a high beam quality laser at 1976 nm is essential for core pumping, which is provided by the Tm^{3+}-doped silica fiber. However, a 790 nm diode-pumped 1976 nm fiber laser increases the complexity of the system and adds an additional energy conversion process which reduces the electro-optical (EO) conversion efficiency, and the core pumping setup is hard for coupling and bad for stability. With the development of the GaSb-based ~2 µm diode [9–12], a single emitter up to 1.4 W and a 19-emitter-bar up to 16 W is available. It is attractive to use a 976 nm and 2 µm laser diode to pump a 3.5 µm fiber laser directly and to operate a clad pump scheme simultaneously, due to its advantages in high integration, accessibility, and stability. With no literature report, the feasibility of using a clad pump scheme to generate a 3.5 µm laser remains to be studied.

2. Numerical Model

Transitions at DWP have been well studied in previous work [13–15]. Those transition processes can be classified as pump absorption, lasing, relaxation, and interionic processes. All processes except relaxation are shown in Figure 1. P_{976} excite ions from level $^4I_{15/2}$ to $^4I_{11/2}$, known as ground state absorption (GSA). The lifetime of level $^4I_{11/2}$ is relatively long and allows GSA to create a virtual ground state (VSA); thus, the transition from level

$^4I_{11/2}$ to level $^4F_{9/2}$ pumped by P_{1976} is called virtual ground state absorption (VGSA). Three excited state absorption (ESA) processes are involved, including ESA_{1a} and ESA_{1b} related to P_{976}, and ESA_2 related to P_{1976}. SE_1 and SE_2 stand for stimulated emission at 2.8 µm and 3.5 µm, respectively. Interionic processes are marked by W_{ijkl} and represent the energy transfer between ions from energy level i and j and the transition to energy level k and l. Four interionic processes have been reported up to now, which are non-radiative, but play a key role in the laser operation.

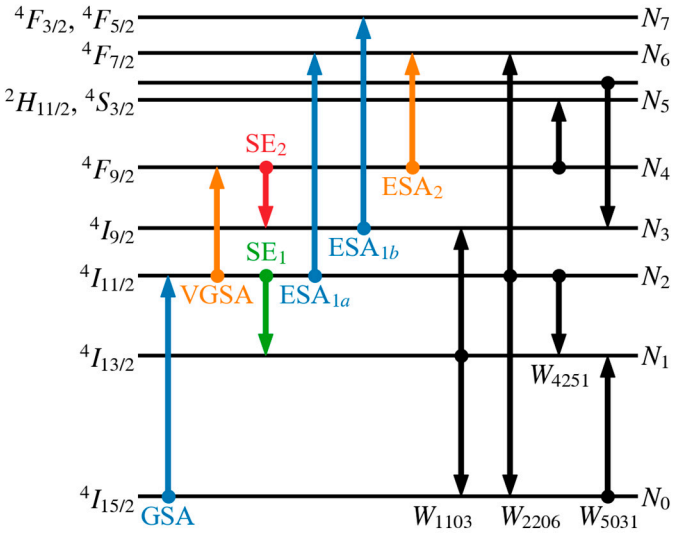

Figure 1. The energy levels of erbium ions and energy transfer processes.

The transition rate from level i to level j during pump absorption processes can be described as:

$$\begin{aligned} R_{ij}(z,t) &= \Gamma \cdot v \cdot G_{ij} \cdot F(z,t) \\ &= \Gamma \cdot v \cdot \left(\sigma_{ij} N_i(z,t) - \sigma_{ji} N_j(z,t)\right) \cdot F(z,t), \end{aligned} \tag{1}$$

where z is the position along the fiber, t represents time, $v = c_0/n_{core}$ is the speed of light inside the fiber core, c_0 is the speed of light in vacuum, n_{core} is the core reflective index, σ_{ij} is the effective cross sections of absorption or emission of a transition from level i to level j, N_i is the particle population of level i, and F is the density of laser photons inside the fiber core. Γ is the mode overlap, representing the power in the mode that overlaps the core. Only the overlapped part of the laser can interact with the Er^{3+} ions. The differences between a core pump and a clad pump are mainly attributed to the different in Γ. The mode overlap of a gaussian beam is given by [16]:

$$\Gamma = 1 - \exp\left(-2\frac{a^2}{\omega^2}\right), \tag{2}$$

$$\omega \approx a \cdot \left(0.65 + \frac{1.619}{V^{3/2}} + \frac{2.879}{V^6}\right), \tag{3}$$

$$V = \frac{2\pi a}{\lambda} \cdot NA, \tag{4}$$

where a is the core radius of the fiber, and NA is the numerical aperture of the fiber. However, for clad pumping, the mode overlap can be estimated by $\Gamma = A_{core}/A_{clad}$, where A_{core} and A_{clad} are the cross-sectional areas of the fiber core and clad, respectively.

The photon density inside the fiber core can be calculated by:

$$F(\nu) = \Gamma(\nu)\frac{P(\nu)n_{core}(\nu)}{A_{core}h\nu c_0}, \tag{5}$$

where P is the laser power, h is the Planck's constant, and ν is the photon frequency. The relaxation rate r_{ij} from level i to level j is given by:

$$r_{ij} = \beta_{ij}/\tau_i, \tag{6}$$

$$\sum_{j=1}^{i-1} \beta_{ij} = 1, \tag{7}$$

where β_{ij} is the branching ratio from level i to level j and τ is the intrinsic lifetime.

There have been four interionic processes reported thus far, three energy-transfer up conversions (ETU), W_{1103}, W_{2206}, and W_{4251}, and one cross relaxation (CR) process, W_{5031}. These processes can be expressed in the rate equations as:

$$R_{1103} = N_1^2 W_{1103}, \tag{8}$$

$$R_{2206} = N_2^2 W_{2206}, \tag{9}$$

$$R_{4251} = N_4 N_2 W_{4251}, \tag{10}$$

$$R_{5031} = N_5 N_0 W_{5031}, \tag{11}$$

For better readability, the transition rate R_{ij} is replaced by the name of the transition process, including R_{02}, R_{24}, R_{43}, R_{21}, R_{26}, R_{37}, R_{46}, replaced by R_{GSA}, R_{VGSA}, R_{SE2}, R_{SE1}, R_{ESA1a}, R_{ESA1b}, R_{ESA2} separately. The full rate equations for population densities, the photonic rate equations, and the boundary conditions are given in Appendix B.

A numerical model was developed in Python to simulate the particle population and laser power behavior of the DWP 3.5 µm erbium-doped fiber laser. For a given situation, the rate equations were solved within one second. The parameters used in the model can be found in [14,15,17]. The model was validated by comparing its results with the measured data reported in [15], as shown in Figure 2. The following simulations had the same fiber parameters, which were 3.4 m of fiber length, 16.5 µm of core diameter, 240 × 260 µm of clad diameter, and 1 mol.% of erbium concentration.

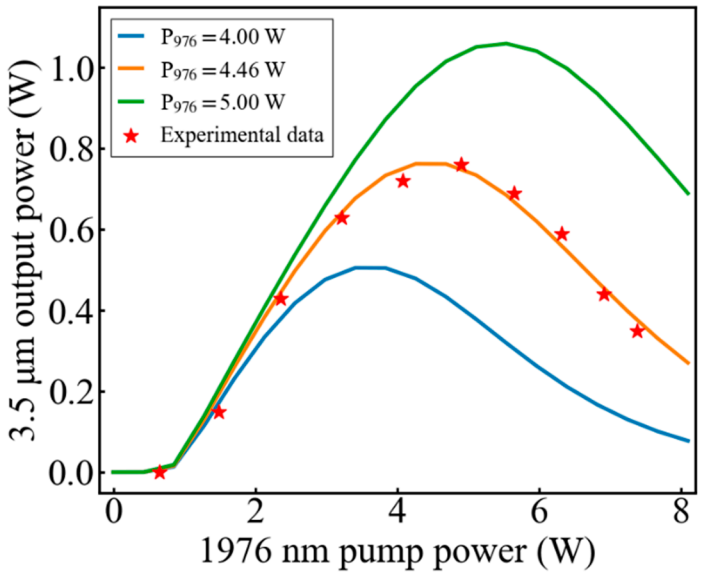

Figure 2. Output power of 3.5 µm laser as a function of power of P_{1976}. Three curves correspond to P_{976} power of 4.0, 4.46, and 5.0 W. Star points correspond to measured data reported in [15] under P_{976} power of 4.46 W.

3. Results and Discussion

3.1. DWCP and Pump Absorbed Rate

Figure 3a shows that by changing the pump mode of the 1976 nm pump from a core pump to a clad pump, the 3.5 µm laser was still available. However, the threshold was much higher, and the slope efficiency was lower, and the DWP scheme showed a saturation phenomenon as the power of P_{1976} increased. Changing the pump mode of P_{1976} from a core pump to a clad pump changed the mode overlap Γ_{1976}. Therefore, the absorbed rate of P_{1976}, α_{1976} was different, given by:

$$\alpha_{1976} = -\Gamma_{1976}(G_{VGSA} + G_{ESA2} + \alpha_{loss}) \cdot P_{1976}, \quad (12)$$

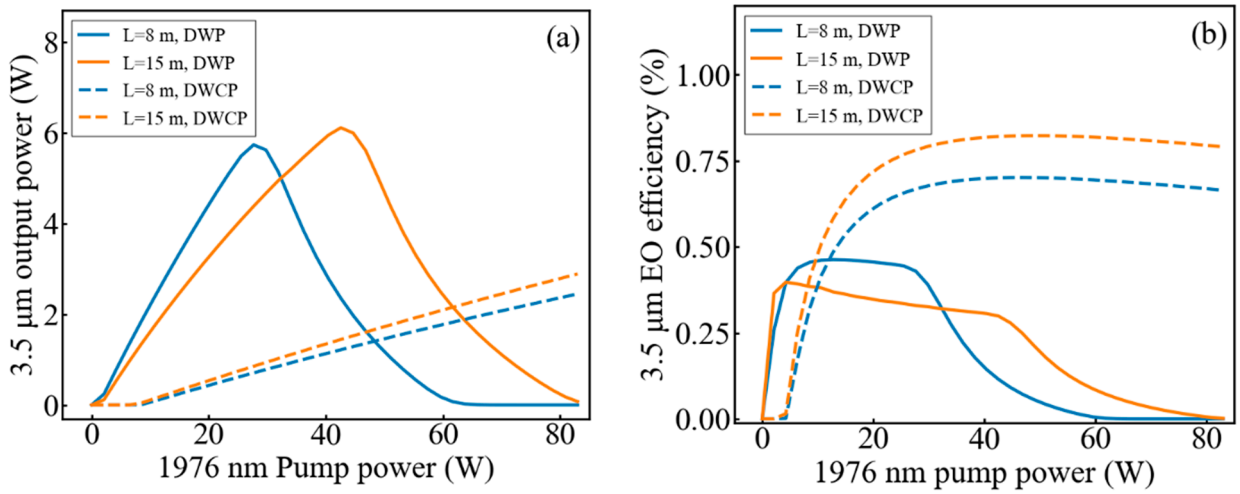

Figure 3. (**a**) Output power of a 3.5 µm laser and (**b**) Electro-optical (EO) efficiency of a 3.5 µm laser as a function of power of P_{1976}. Simulated at P_{976} power of 10 W for the dual-wavelength pump (DWP) and dual-wavelength-clad-pumped (DWCP) schemes.

The difference of Γ_{1976} and α_{1976} between these two schemes can explain the different optimization behaviors. The P_{1976} was absorbed much slower in the DWCP setup; thus, the stimulation threshold was higher, and the slope efficiency was lower. The saturation phenomenon called quenching was caused by the increasing ESA_2 process that depleted the Er^{3+} ions in level $^4F_{9/2}$ [15]. For a certain fiber, the quenching point is affected by the power of P_{976}. Different powers of P_{976} yield different output power curves with similar tendency but different quenching points. Thus, in this paper, P_{976} was set as a typical power of 5 W, except in Figure 3. Since the power of P_{1976} was calculated up to 80 W, a matched P_{976} of 10 W was applied. The result showed that under the DWP scheme, quenching was more significant on a shorter fiber. For a longer fiber, quenching was delayed but the slop efficiency was reduced. Whereas under the DWCP scheme, considering the limited pump load capacity of the fluoride fiber, quenching was not a thing to be concerned about. This was because in this situation, quenching happened when P_{1976} went beyond 600 W. Figure 3a also shows that using a fiber with a proper length is a way to compensate for the low slope efficiency when using the DWCP scheme. The effect of fiber length was investigated in detail and is shown in the next section. Referring to the result in Figure 3a, the following simulations used 5–20 W of P_{1976} for the DWP scheme and 20–80 W for DWCP to make the output power compatible.

Figure 3b shows that the DWCP scheme achieved a higher EO efficiency than the DWP scheme. EO efficiency was calculated as the output of the 3.5 µm laser power divided by the total input electrical power of both pumps. The EO efficiency of the 2 µm laser diode was from [12], and 15% was used in this simulation. Moreover, the EO efficiency of the 2 µm fiber laser was measured from a homemade Tm^{3+} fiber laser pumped by a 790 nm

commercial laser diode, which was about 2.1%. The 1976 nm laser diode had a higher EO efficiency but a lower absorption rate, and it turned out that a higher EO efficiency was achievable in the DWCP scheme.

3.2. Fiber Length

Figure 4a shows that as the fiber length increased, the output power of the 3.5 µm laser increased and then decreased, and the best length of fiber was strongly related to the power of P_{1976}. Under the current pump power level, a fiber of 5–15 m long was proper for the core pumped scheme. However, for the DWCP situation in Figure 4b, a fiber of about 15 m long was good for different pump powers. This was caused by the different pump absorbed rates in different schemes. For the DWP scheme, P_{1976} was absorbed much faster than P_{976} when propagating in the fiber, as shown in Figure 4c. Thus, at the latter part of the fiber, a 1976 nm laser did not have enough power, making the gain of the 3.5 µm laser smaller than the loss, and the output power decreased. For a different P_{1976} power, the pump absorbed rates were similar, so the higher the power of P_{1976} was, the longer the fiber needed to deplete the pump. However, for the DWCP scheme, the α_{1976} was much lower than that in the core pumped situation. In this case P_{976} was absorbed to a lower level first and caused the gain of the 3.5 µm laser to be smaller than the loss, as Figure 4d shows. The absorbed rate of P_{976} did not change significantly along the power of P_{976}, therefore this 15-m-long fiber would be suitable for a wide range of pump configurations. It is worth noticing that in the DWCP scheme, there was a significant amount of residual P_{1976}. Because most 1976 nm lasers are transmitted in fiber cladding, which means they do not interact with Er^{3+} ions, it is necessary to have a higher power level of P_{1976} than that in the DWP scheme in order to maintain the gain of the fiber. In Figure 4c,d, 10 W of P_{976} was chosen to show the drain of P_{1976} while 5 W of P_{976} was still used in other parts of this paper for consistency.

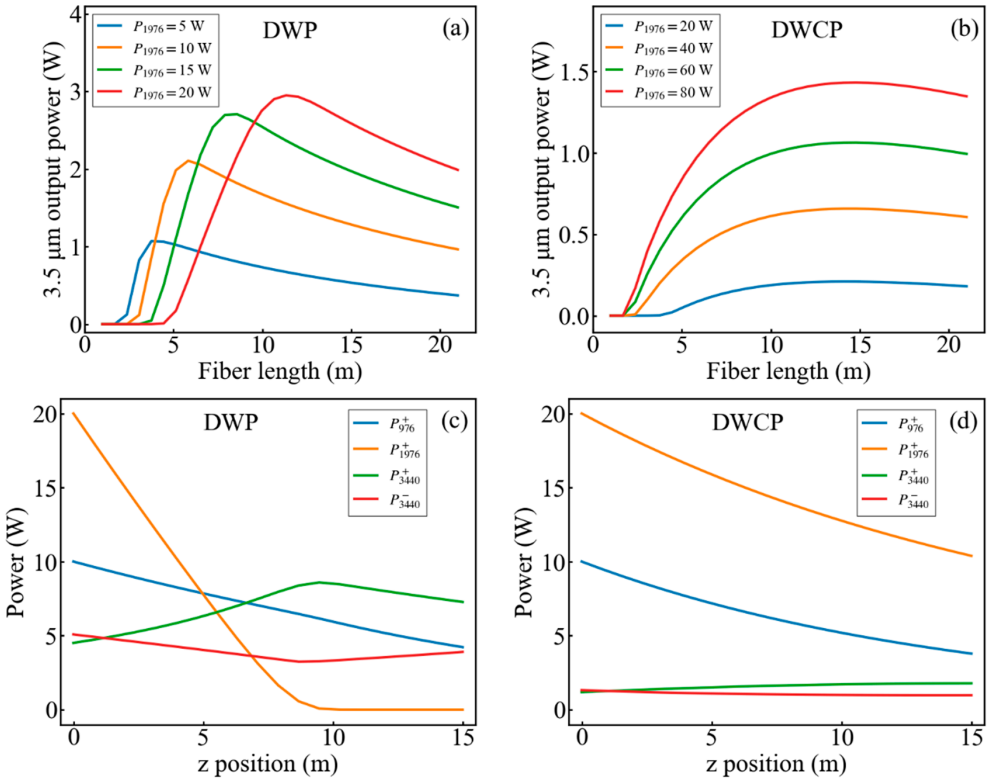

Figure 4. Output power of a 3.5 µm laser as a function of fiber length at 5 W of P_{976} and different powers of P_{1976} under (**a**) the DWP scheme and (**b**) the DWCP scheme. Laser power distribution of P_{976}, P_{1976}, and the 3.5 µm laser under conditions of P_{976} power 10 W, P_{1976} power 20 W, fiber length 15 m (**c**) DWP scheme, (**d**) DWCP scheme.

3.3. Core Diameter

The most significant difference between the DWP and DWCP scheme was the mode overlap of P_{1976}, Γ_{1976}. Moreover, Γ_{1976} was mostly related to the fiber core diameter, so optimizing the fiber core diameter in these two schemes was expected to be quite different. As shown in Figure 5a,b, the optimum points of the DWP scheme were strongly related to the power of P_{1976}, whereas the DWCP scheme was suitable for a larger core diameter, and the optimum points were of lower relevance to the fiber core diameter. These differences can be explained by the different slope of Γ_{1976} versus the fiber core diameter plotted in Figure 5c, with the dotted part corresponding to the multi-mode range that (2) was no longer accurate. Γ_{1976} at the DWCP scheme was overall much lower, and its slope versus fiber core diameter increased as the diameter increased, whereas the slope of another curve decreased. For a certain power of pump, a larger fiber core diameter led to a larger Γ_{1976}, and therefore a larger P_{1976} absorbed rate. Continuously increasing the fiber core diameter after the pump lasers absorbed too much made the output power decrease. So, the Γ_{1976} variety decided the pump absorbed rate and yielded the output power behavior.

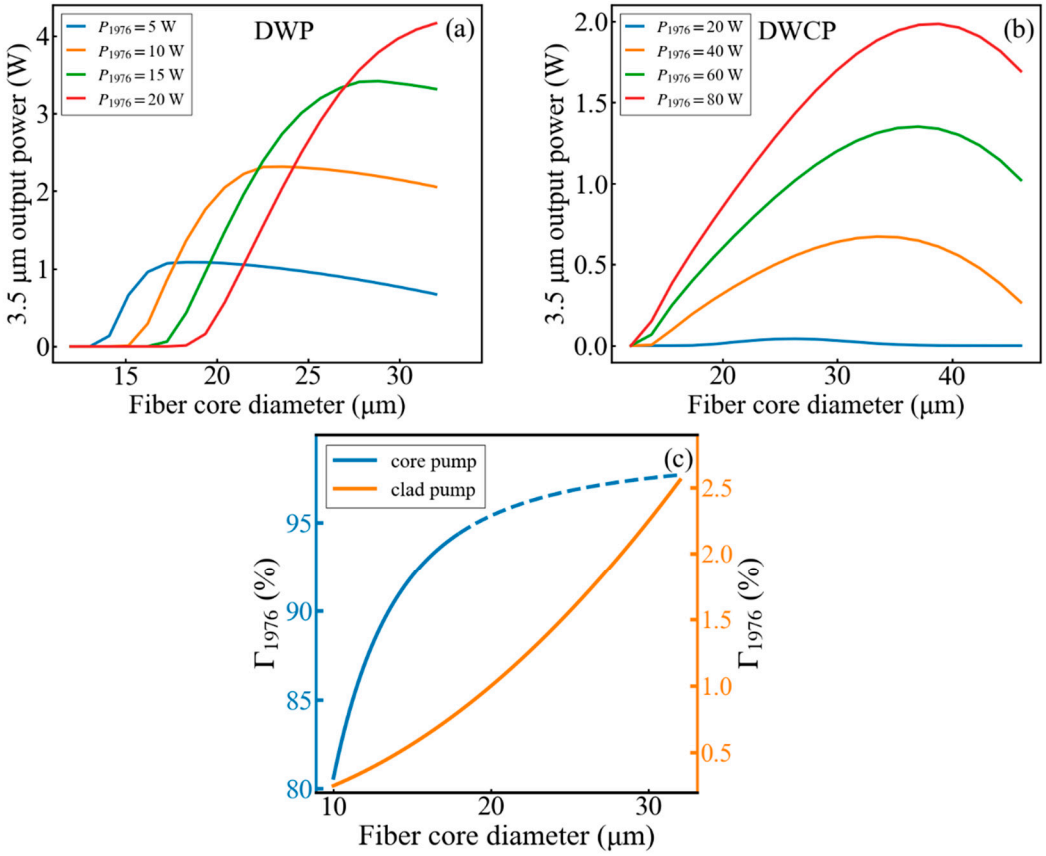

Figure 5. Output power of a 3.5 μm laser as a function of the fiber core diameter at 5 W of P_{976} and a different power of P_{1976} under (**a**) the DWP scheme and (**b**) the DWCP scheme. (**c**) Γ_{1976} as a function of the fiber core diameter at the DWP scheme and the DWCP scheme.

3.4. Reflectivity of Resonant Cavity

The 3.5 μm fiber laser utilized an output coupler (OC) or a fiber bragger grating (FBG) to control the reflectivity of the resonant cavity. In this simulation, OC reflectivity was used to represent the reflectivity of the non-high-reflective side of the cavity. Figure 6 shows how the output power changed with the OC reflectivity. The optimum point for the DWP scheme turned out to be lower than the DWCP scheme. Since the α_{1976} was very high in the DWP scheme, a lower OC reflectivity was enough to make full use of the P_{1976}. The optimum point of OC reflectivity was higher as the power of P_{1976} increased in the DWP

scheme but lower in the DWCP scheme. Under the DWP scheme, for a certain length of fiber, a higher OC reflectivity led to a higher 3.5 μm laser energy inside the fiber, which consumed excited state ions in level 4 and contributed to the absorption of P_{1976}. Thus, a higher OC reflectivity means a higher α_{1976}, and for a higher power of P_{1976}, it takes a higher OC reflectivity to deplete P_{1976}. However, for the DWCP scheme, as what happened in the fiber length optimization, P_{976} was depleted before P_{1976}. For a settled 5 W of P_{976}, the higher the power of P_{1976} was, the easier P_{976} was depleted. So, the best OC reflectivity is lower as the power of P_{1976} increases.

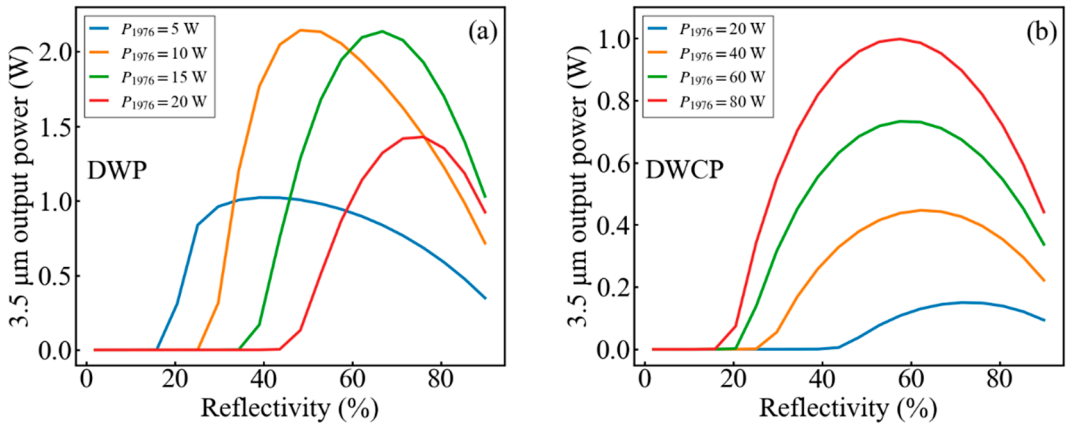

Figure 6. Output power of a 3.5 μm laser as a function of output coupler (OC) reflectivity at 5 W of P_{976} and different powers of P_{1976} under (**a**) the DWP scheme and (**b**) the DWCP scheme.

3.5. Dopant Concentration

The dopant concentration of the fiber laser is more complex than other parameters. A higher rear-earth-dopant concentration can increase the gain of the fiber, increase the slope efficiency, and therefore decrease the fiber length and reduce the fiber cost. However, a higher dopant concentration also leads to more heat generation and increases the probability of energy transfer processes. Heat generation and interionic processes were investigated and are shown in Figure 7. From Figure 7a,b, it is clear that regardless of other effects, a higher erbium concentration was definitely better for a high power output. To calculate the effect of the erbium concentration on the core temperature, the method given in [18,19] was utilized and the result is shown in Figure 7c. The DWCP scheme was feasible for much a higher erbium concentration in terms of heat generation. This temperature excursion calculated the heat caused by energy transfer processes at lasing. Considering the P_{1976} was focused on the clad rather than core of the fiber, the pump power density was lower in the DWCP scheme which was also good for heat dissipation and high-power generation.

Figure 7d shows the effect of interionic processes, that is, W_{1103}, W_{2206}, W_{4251}, and W_{5031} in this fiber laser. The higher erbium concentration made it easier for ions to interact with each other. To investigate how these processes affected the output power of the 3.5 μm laser, the rates of these four processes were tuned higher separately and together and then compared with a normal fiber. The result shows W_{1103} and W_{5031} were positive for 3.5 μm lasing, whereas W_{2206} and W_{4251} were negative. As the interionic processes enhanced together, the total effect was negative. In conclusion, erbium concentration cannot be given a simple optimized number, and the choice of concentration should consider the cooling capacity and measured power curve, but the appropriate concentration value of the DWCP scheme was clearly higher than that of the DWP scheme.

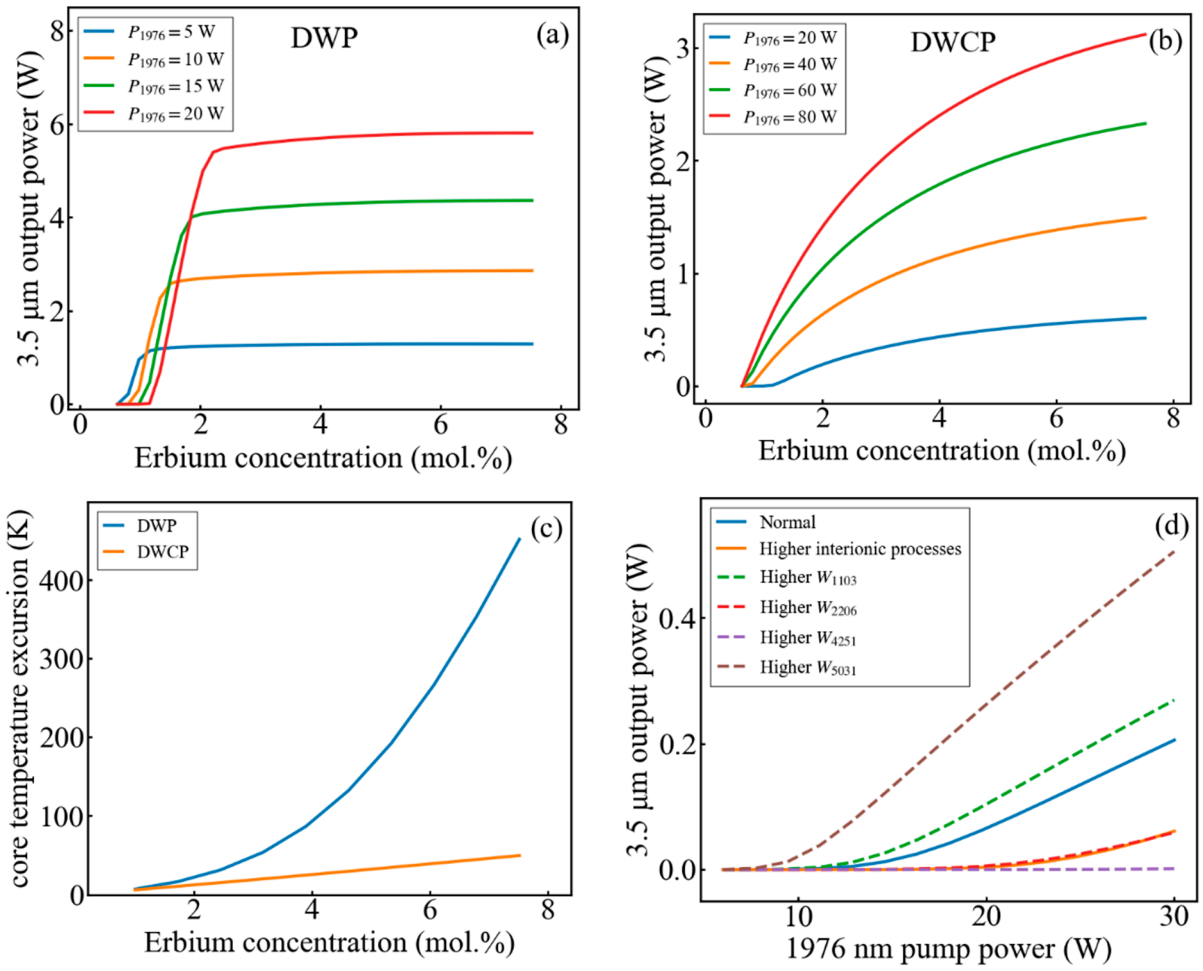

Figure 7. Output power of a 3.5 μm laser as a function of erbium concentration at 5 W of P_{976} and different powers of P_{1976} under (**a**) the DWP scheme and (**b**) the DWCP scheme. (**c**) Core temperature excursion as a function of erbium concentration, at 5 W of P_{976} power and 30W of P_{1976} power. The temperature is simulated sectionally at the centre of the fiber core and axially at the pump injection facet. (**d**) Output power of a 3.5 μm laser as a function of P_{1976} power, simulated at 5 W of P_{976}. Label "normal" corresponds to the simulation with interionic processes rates of 1 mol.% erbium concentration as in [15]. Dotted lines correspond to the simulation with a higher individual interionic process. Label "higher interionic processes" corresponds to the simulation with all interionic processes rates tuned higher.

4. Conclusions

In summary, we demonstrated a new pump scheme for a 3.5 μm erbium-doped fluoride fiber laser, DWCP. The EO efficiency was better than the traditional DWP scheme, whereas the slop efficiency decreased, and the lasing threshold increased. Since the difference in the absorbed rate of P_{1976}, the DWCP scheme is more suitable for a longer fiber length, a larger fiber core diameter, a larger OC reflectivity, and a higher erbium concentration compared to the DWP scheme. This work provides the theoretical foundations for using laser diodes to pump a 3.5 μm fiber laser.

Author Contributions: Conceptualization, K.C. and X.Z.; methodology, K.C. and X.Z.; software, K.C.; validation, K.C.; formal analysis, K.C., X.Z., L.W. (Lijie Wang), Y.W., H.L. and C.T.; investigation, K.C., X.Z., L.W. (Lijie Wang), Y.W. and H.L.; resources, C.T. and L.W. (Lijun Wang); data curation, K.C.; writing—original draft preparation, K.C.; writing—review and editing, K.C., X.Z. and C.T.; visualization, K.C.; supervision, C.T. and L.W. (Lijun Wang); project administration, C.T.; funding acquisition, C.T. All authors have read and agreed to the published version of the manuscript.

Funding: This research was funded by the National Natural Science Foundation of China, grant number 61790584, the National Science Fund for Distinguished Young Scholars, grant number 62025506, and the CAS Youth Innovation Promotion Association, grant number 2018249.

Institutional Review Board Statement: Not applicable.

Data Availability Statement: Not applicable.

Acknowledgments: K.C. thanks Regan for helping with the grammar. Authors would like to thank our anonymous reviewers for the helpful and detailed comments and suggestions.

Conflicts of Interest: The authors declare no conflict of interest.

Appendix A

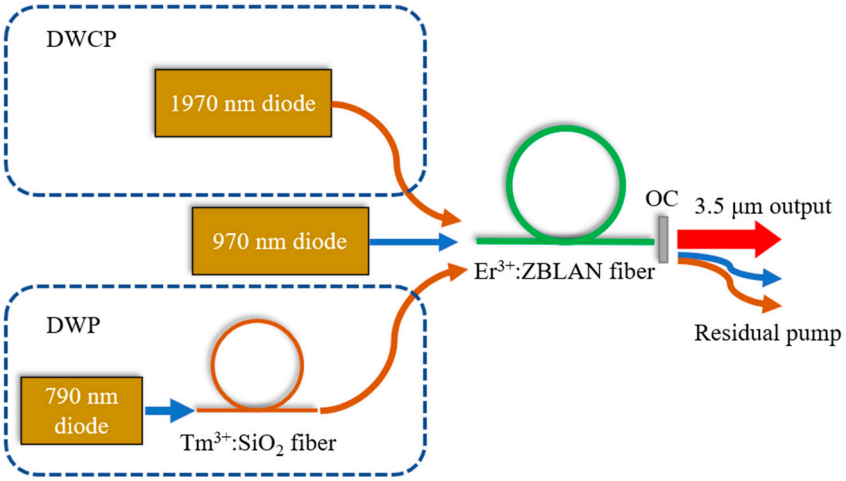

Figure A1. Schematic diagram of a 3.5 μm fiber laser for the DWP and DWCP schemes, OC for output coupler.

Appendix B

The rate equations for population densities are as follows:

$$\frac{dN_6(z,t)}{dt} = -\sum_{i=0}^{5} r_{6i}N_6 + R_{ESA_{1a}} + R_{ESA_{1b}} + R_{ESA_2} + R_{2206}, \tag{A1}$$

$$\frac{dN_5(z,t)}{dt} = r_{65}N_6 - \sum_{i=0}^{4} r_{5i}N_5 + R_{4251} - R_{5031}, \tag{A2}$$

$$\frac{dN_4(z,t)}{dt} = \sum_{i=5}^{6} r_{i4}N_i - \sum_{i=0}^{3} r_{4i}N_4 - R_{ESA_2} + R_{VSA} - R_{SE_2} - R_{4251}, \tag{A3}$$

$$\frac{dN_3(z,t)}{dt} = \sum_{i=4}^{6} r_{i3}N_i - \sum_{i=0}^{2} r_{3i}N_3 - R_{ESA_{1b}} + R_{SE_2} + R_{1103} + R_{5301}, \tag{A4}$$

$$\frac{dN_2(z,t)}{dt} = \sum_{i=3}^{6} r_{i2}N_i - \sum_{i=0}^{1} r_{2i}N_2 + R_{GSA} - R_{ESA_{1a}} - R_{VSA} - R_{SE1} - 2R_{2206} - R_{4251}, \tag{A5}$$

$$\frac{dN_1(z,t)}{dt} = \sum_{i=2}^{6} r_{i1}N_i - r_{10}N_1 + R_{SE1} - 2R_{1103} + R_{4251} + R_{5031}, \tag{A6}$$

$$\frac{dN_0(z,t)}{dt} = \sum_{i=1}^{6} -R_{GSA} + R_{1103} + R_{2206} - R_{5031}, \tag{A7}$$

$$N(z,t) = \sum_{i=0}^{6} N_i(z,t), \tag{A8}$$

The photonic rate equations are given by:

$$\pm \frac{dP_{976}^{\pm}(z,t)}{dz} = \pm\Gamma_{976}(G_{ESA1a} - G_{GSA} - G_{ESA1b})P_{976}^{\pm}(z,t) \pm R_{loss976}P_{976}^{\pm}(z,t), \tag{A9}$$

$$\pm \frac{dP_{1976}^{\pm}(z,t)}{dz} = \pm\Gamma_{1976}(G_{VSA} - G_{ESA2})\ P_{1976}^{\pm}(z,t)\ \pm R_{loss1976}P_{1976}^{\pm}(z,t), \tag{A10}$$

$$\pm \frac{dP_{l1}^{\pm}(z,t)}{dz} = \pm\Gamma_{l1}G_{SE1}P_{l1}^{\pm}(z,t) \pm R_{lossl1}P_{l1}^{\pm}(z,t), \tag{A11}$$

$$\pm \frac{dP_{l2}^{\pm}(z,t)}{dz} = \pm\Gamma_{l2}G_{SE2}P_{l2}^{\pm}(z,t) \pm R_{lossl2}P_{l2}^{\pm}(z,t), \tag{A12}$$

where P_{976} and P_{1976} are the powers of the 976 nm and 1976 nm pump. P_{l1} and P_{l2} are the powers of the 2800 nm and 3500 nm laser light. R_{loss} is the background loss coefficient. The boundary conditions are given by:

$$P_{976}^{+}(0) = P_{976}^{-}(0)R_{976} + P_{976}, \tag{A13}$$

$$P_{1976}^{+}(0) = P_{1976}^{-}(0)R_{1976} + P_{1976}, \tag{A14}$$

$$P_{l1}^{+}(0) = P_{l1}^{-}(0)R_{l1}, \tag{A15}$$

$$P_{l2}^{+}(0) = P_{l2}^{-}(0)R_{l2}, \tag{A16}$$

$$P_{976}^{-}(L) = P_{976}^{+}(L)R'_{976}, \tag{A17}$$

$$P_{1976}^{-}(L) = P_{1976}^{+}(L)R'_{1976}, \tag{A18}$$

$$P_{l1}^{-}(L) = P_{l1}^{+}(L)R'_{l1}, \tag{A19}$$

$$P_{l2}^{-}(L) = P_{l2}^{+}(L)R'_{l2}, \tag{A20}$$

where R and R' are the reflectivities of the laser cavity at the $z = 0$ and $z = L$ positions. L is the length of the fiber.

References

1. Jackson, S.D.; Jain, R.K. Fiber-based sources of coherent MIR radiation: Key advances and future prospects (invited). *Opt. Express* **2020**, *28*, 30964–31019. [CrossRef] [PubMed]
2. Bekman, H.H.P.T.; Heuvel, J.C.V.D.; van Putten, F.J.M.; Schleijpen, R. Development of a mid-infrared laser for study of infrared countermeasures techniques. In Proceedings of the European Symposium on Optics and Photonics for Defence and Security, London, UK, 25–28 October 2004; pp. 27–38.
3. Walsh, B.M.; Lee, H.R.; Barnes, N.P. Mid infrared lasers for remote sensing applications. *J. Lumin* **2016**, *169*, 400–405. [CrossRef]
4. Kottmann, J.; Grob, U.; Rey, J.M.; Sigrist, M.W. Mid-Infrared Fiber-Coupled Photoacoustic Sensor for Biomedical Applications. *Sensors* **2013**, *13*, 535–549. [CrossRef] [PubMed]
5. Henderson-Sapir, O.; Munch, J.; Ottaway, D.J. Mid-infrared fiber lasers at and beyond 35 μm using dual-wavelength pumping. *Opt. Lett.* **2014**, *39*, 493–496. [CrossRef]
6. Fortin, V.; Maes, F.; Bernier, M.; Bah, S.T.; D'Auteuil, M.; Vallée, R. Watt-level erbium-doped all-fiber laser at 344 μm. *Opt. Lett.* **2016**, *41*, 559–562. [CrossRef] [PubMed]
7. Maes, F.; Fortin, V.; Bernier, M.; Vallée, R. 56 W monolithic fiber laser at 355 μm. *Opt. Lett.* **2017**, *42*, 2054–2057. [CrossRef] [PubMed]
8. Lemieux-Tanguay, M.; Fortin, V.; Boilard, T.; Paradis, P.; Maes, F.; Talbot, L.; Vallée, R.; Bernier, M. 15 W monolithic fiber laser at 3.55 μm. *Opt. Lett.* **2022**, *47*, 289–292. [CrossRef] [PubMed]
9. Reboul, J.R.; Cerutti, L.; Rodriguez, J.B.; Tournié, E.; Grech, P. Continuous-wave operation above room temperature of GaSb-based laser diodes grown on Si. *Appl. Phys. Lett.* **2011**, *99*, 121113. [CrossRef]
10. Liao, Y.; Zhang, Y.; Yang, C.; Huang, S.; Chai, X.; Wang, G.; Xu, Y.; Ni, H.; Niu, Z. High-power, high-efficient GaSb-based quantum well laser diodes emitting at 2 μm. *J. Infrared Millim. Waves* **2016**, *35*, 672–675. [CrossRef]

11. Yang, C.-A.; Xie, S.-W.; Zhang, Y.; Shang, J.-M.; Huang, S.-S.; Yuan, Y.; Shao, F.-H.; Zhang, Y.; Xu, Y.-Q.; Niu, Z.-C. High-power, high-spectral-purity GaSb-based laterally coupled distributed feedback lasers with metal gratings emitting at 2 μm. *Appl. Phys. Lett.* **2019**, *114*, 021102. [CrossRef]
12. Xie, S.-W.; Zhang, Y.; Yang, C.-A.; Huang, S.-S.; Yuan, Y.; Zhang, Y.; Shang, J.-M.; Shao, F.-H.; Xu, Y.-Q.; Ni, H.-Q.; et al. High performance GaSb based digital-grown InGaSb/AlGaAsSb mid-infrared lasers and bars. *Chin. Phys. B* **2019**, *28*, 014208. [CrossRef]
13. Henderson-Sapir, O.; Jackson, S.; Ottaway, D.J. Versatile and widely tunable mid-infrared erbium doped ZBLAN fiber laser. *Opt. Lett.* **2016**, *41*, 1676–1679. [CrossRef] [PubMed]
14. Henderson-Sapir, O.; Munch, J.; Ottaway, D.J. New energy-transfer upconversion process in Erˆ3+: ZBLAN mid-infrared fiber lasers. *Opt. Express* **2016**, *24*, 6869–6883. [CrossRef] [PubMed]
15. Maes, F.; Fortin, V.; Bernier, M.; Vallee, R. Quenching of 3.4 μm Dual-Wavelength Pumped Erbium Doped Fiber Lasers. *IEEE J. Quantum Electron.* **2017**, *53*, 1–8. [CrossRef]
16. Marcuse, D. Gaussian approximation of the fundamental modes of graded-index fibers. *J. Opt. Soc. Am.* **1978**, *68*, 103–109. [CrossRef]
17. Malouf, A.; Henderson-Sapir, O.; Gorjan, M.; Ottaway, D.J. Numerical Modeling of 3.5 μm Dual-Wavelength Pumped Erbium-Doped Mid-Infrared Fiber Lasers. *IEEE J. Quantum Electron.* **2016**, *52*, 1–12. [CrossRef]
18. Li, J.; Luo, H.; Liu, Y.; Zhang, L.; Jackson, S.D. Modeling and Optimization of Cascaded Erbium and Holmium Doped Fluoride Fiber Lasers. *IEEE J. Sel. Top. Quantum Electron.* **2013**, *20*, 15–28. [CrossRef]
19. Gorjan, M.; Marincek, M.; Copic, M. Pump absorption and temperature distribution in erbium-doped double-clad fluoride-glass fibers. *Opt. Express* **2009**, *17*, 19814–19822. [CrossRef] [PubMed]